

TABLE II: Estimation of the  $\Delta S^\ddagger(298)$  for Reaction 1 Using the Bent TS Model (Figure 3)

degrees of freedom	$\Delta S^\ddagger(\text{diff})$ , eu
translational: $\Delta S_{tr} = \frac{3}{2}R \ln(M^*/M) = \frac{3}{2}R \ln(125/90)$	1.0
rotational: $\Delta S_{rot} = \frac{1}{2}R \ln((I_A I_B I_C)^*/I_A I_B I_C) = \frac{1}{2}R \ln(19.5)$	3.0
electronic: $\Delta S_{el} = R \ln(2S + 1) = R \ln 2$	1.4
symmetry: $\Delta S_s = R \ln(\sigma/\sigma^*) = R \ln 2$	1.4
internal rotations:	
about C...H bond, $S_f(I_r = 50.8 \text{ amu } \text{Å}^2)$	8.5
about C-N bond, $\Delta S_f = \frac{1}{2}R \ln(I_r^*/I_r)$	3.1
about N-N bond, $\Delta S_f = \frac{1}{2}R \ln(I_r^*/I_r)$	0.3
vibrational: $\nu(\text{C-H}), 3000 \text{ cm}^{-1} \rightarrow \nu(\text{C}\cdots\text{H}), 2100 \text{ cm}^{-1}$	rc
$\nu_b(\text{H}-\overset{\curvearrowright}{\text{C}}-\text{N}), 1050 \text{ cm}^{-1} \rightarrow \nu_b(\text{H}\cdots\overset{\curvearrowright}{\text{C}}-\text{N}), 750 \text{ cm}^{-1}$	0.3
$(2)\nu_b(\text{H}-\overset{\curvearrowright}{\text{C}}-\text{H}), 1450 \text{ cm}^{-1} \rightarrow (2)\nu_b(\text{H}\cdots\overset{\curvearrowright}{\text{C}}-\text{H}), 1000 \text{ cm}^{-1}$	0.2
$\rightarrow (2)\nu_b(\text{C}\cdots\text{H}\cdots\text{Cl}), 700 \text{ cm}^{-1}$	0.6
$\rightarrow \nu(\text{H}\cdots\text{Cl}), 2100 \text{ cm}^{-1}$	0
	total 19.8
$\Delta S^\ddagger(298) = 19.8 - 39.5 = -19.7 \text{ eu}$	

the conventional transition-state theory (bent model).

Therefore, our experimental findings suggest that the approach of Cl atoms relative to the C-H bond involves a bent structure. The nonlinear approach of Cl may be normal considering that the incoming Cl, while approaching a methyl group, is attracted by all three H atoms and is repelled by the O and N atoms. Therefore, it is oriented in such a way (inclined to the C-H axis) that it can form a covalent bond with one H atom, compensating for the repulsion by the O and N atoms and the attraction by the other H atoms.

The  $A$  factor obtained ( $10^{-9.84} \text{ cm}^3 \text{ molecule}^{-1} \text{ s}^{-1}$ ) is very close to the value  $10^{-9.76} \text{ cm}^3 \text{ molecule}^{-1} \text{ s}^{-1}$ , reported for the reaction of Cl with dimethyl ether.<sup>12</sup> Furthermore, it has been found that

(12) Michael, J. V.; Nava, D. F.; Payne, W. A.; Stief, L. J. *J. Chem. Phys.* 1979, 70, 3652.

in most reactions of Cl with oxygenated hydrocarbons having C-H bond strengths less than 95 kcal/mol there is no activation energy.<sup>13</sup> Since our reaction has an activation energy of 1.2 kcal/mol, there is strong evidence that the C-H bond strength in DMNA is higher than 95 kcal/mol and most probably has a value between methane ( $104 \pm 1 \text{ kcal/mol}$ ) and ethane ( $98 \pm 1 \text{ kcal/mol}$ ).<sup>14</sup> Thus, the estimated value of 95 kcal/mol obtained by theoretical calculations<sup>15</sup> is rather low.

The secondary reaction of Cl with  $\text{CH}_3\text{N}=\text{CH}_2$  has been found to have a rate constant of  $1.5 \times 10^{-12} \text{ cm}^3 \text{ molecule}^{-1} \text{ s}^{-1}$  at 303 K, an order of magnitude lower than that of  $k_1$ , and presented no complications to our experiments. The analogous reaction of Cl with  $\text{CH}_3\text{CH}=\text{CH}_2$  has a much higher rate constant of  $2.68 \times 10^{-10} \text{ cm}^3 \text{ molecule}^{-1} \text{ s}^{-1}$  at 295 K.<sup>16</sup> This is probably due to the fact that the imine molecule possesses a rather large negative charge around the nitrogen atom that repels the approaching Cl atom and reduces the reactive cross section.

Finally, this fast reaction of Cl with dimethylnitramine can play a significant role in the stability of nitramines. Small concentrations of Cl atoms over nitramine samples will decompose them to  $\text{NO}_2$  and the corresponding imine. This chemical decomposition of nitramines has been also observed in the infrared multiphoton decomposition of dimethylnitramine in the presence of  $\text{Cl}_2$  molecules.<sup>17</sup>

**Acknowledgment.** Y.L. acknowledges the financial support by the Institute of Electronic Structure and Laser, F.O.R.T.H.

**Registry No.** Chlorine (atomic), 22537-15-1; dimethylnitramine, 4164-28-7.

(13) Michael, J. V.; Nava, D. F.; Payne, W. A.; Stief, L. J. *J. Chem. Phys. Lett.* 1981, 77, 110.

(14) Golden, D. M.; Benson, S. W. *Chem. Rev.* 1969, 69, 125.

(15) Melius, C. F.; Binkley, J. S. Thermochemistry of the Decomposition of Nitramines in the Gas Phase. In *Proceedings of the 21st Symposium (International) on Combustion*; The Combustion Institute: Pittsburgh, 1986; p 1953.

(16) Wallington, T. J.; Skewes, L. M.; Siegl, W. O. *J. Photochem. Photobiol. A* 1988, 45, 167.

(17) Lazarou, Y. G.; Papagiannakopoulos, P. *J. Phys. Chem.* 1990, 94, 7114.

## Kinetic and Mechanistic Study of $\text{X} + \text{ClOCl} \rightarrow \text{Products}$ ( $\text{X} = \text{Br}, \text{Cl}, \text{F}, \text{O}, \text{OH}, \text{N}$ ) over the Temperature Range 240–373 K

Philip S. Stevens\*<sup>†</sup> and James G. Anderson

Department of Chemistry and Department of Earth and Planetary Sciences, Harvard University, Cambridge, Massachusetts 02138 (Received: May 8, 1991; In Final Form: October 24, 1991)

The rate constants for the reactions of  $\text{X} + \text{ClOCl} \rightarrow \text{products}$  for  $\text{X} = \text{Br}, \text{Cl}, \text{F}, \text{O}, \text{OH}$ , and  $\text{N}$  have been measured over the temperature range 230–400 K. The rate constants are (in units of  $\text{cm}^3 \text{ molecule}^{-1} \text{ s}^{-1}$ ) as follows:  $(2.1 \pm 0.2) \times 10^{-11} \exp[(-425 \pm 30)/T]$  for  $\text{Br} + \text{ClOCl}$ ;  $(6.0 \pm 0.6) \times 10^{-11} \exp[(127 \pm 30)/T]$  for  $\text{Cl} + \text{ClOCl}$ ;  $(1.5 \pm 0.5) \times 10^{-10} \exp[(-47 \pm 94)/T]$  for  $\text{F} + \text{ClOCl}$ ;  $(1.3 \pm 0.8) \times 10^{-11} \exp[(-510 \pm 30)/T]$  for  $\text{O} + \text{ClOCl}$ ;  $(1.7 \pm 0.8) \times 10^{-12} \exp[(420 \pm 170)/T]$  for  $\text{OH} + \text{ClOCl}$ ; and  $k^{298} < 6 \times 10^{-15}$  for  $\text{N} + \text{ClOCl}$ . The rate constants for  $\text{X} = \text{Br}, \text{Cl}, \text{F}$ , and  $\text{N}$  are found to correlate with the electron affinity of the attacking radical, suggesting that the mechanism for these reactions involves the partial transfer of an electron from  $\text{ClOCl}$  to  $\text{X}$ , and the activation energy for reaction is determined by the ability of the transition state to accommodate the shift in electron density. This trend is similar to that found for a number of non-hydrogen abstraction reactions ( $\text{X} + \text{ClNO}, \text{O}_3, \text{Cl}_2$ ), where the reactivity scales with the quantity  $\text{IP}(\text{molecule}) - \text{EA}(\text{radical})$ , where  $\text{IP}$  refers to the ionization potential and  $\text{EA}$  the electron affinity. The reactions of  $\text{O}$  and  $\text{OH}$  with  $\text{ClOCl}$  are significantly faster than predicted by the trend, suggesting that the electron-transfer mechanism is not the only driving force in these reactions, which may involve long-range attractive forces leading to stable intermediates.

### Introduction

In recent years, the thermal rate constants for a number of bimolecular reactions have been shown to display trends with

observable properties of the reactants.<sup>1-3</sup> By examining the nature of these observables, it was shown that the height of the potential

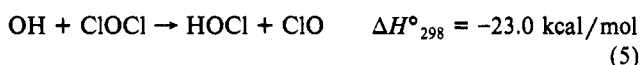
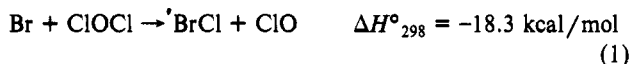
<sup>†</sup> Present address: Department of Meteorology, The Pennsylvania State University, University Park, PA 16802.

(1) Abbatt, J. P. D.; Toohey, D. W.; Fenter, F. F.; Stevens, P. S.; Brune, W. H.; Anderson, J. G. *J. Phys. Chem.* 1989, 93, 1022.

barrier for these reactions depends on the energetics and degree of overlap of the Frontier orbitals of the reactants. Information about the potential-energy surface governing the reaction is thus gained from an examination of the thermal rate data, creating a bridge between the macroscopic measurements and the interactions at the molecular level. Because these thermal rate experiments are easily applied to a variety of reactions, this empirical method provides a unique approach toward understanding the fundamentals of chemical reactivity.

In the case of non-hydrogen atom abstraction reactions, there is a strong correlation of reactivity with the reactants' ability to accept and donate electrons, corresponding to the electron affinity (EA) and the ionization potential (IP) of the reactants. Since a chemical reaction involves the motion of electrons from one reactant to another, it is not surprising that the reactivity of these systems correlates with the quantity IP(electron donor) - EA(electron acceptor).<sup>1-6</sup> This correlation implies that the mechanism for these reactions involves electron delocalization from the highest occupied molecular orbital (HOMO) of the reactant with the lower IP to the lowest unoccupied molecular orbital (LUMO) of the other reactant. Reactants with lower values of IP - EA are more reactive than those with higher values of IP - EA, suggesting that the height of the potential-energy barrier governing reactivity is controlled by the extent of electron delocalization. The lower the IP of one reactant (the greater electron-donating ability) and the higher the EA of the other (the greater electron-accepting ability), the higher the propensity for electron delocalization in the region of the transition state.

The strong correlation of this trend for reactions involving ClNO,<sup>1</sup> O<sub>3</sub>,<sup>2</sup> and YZ<sup>3</sup> (YZ = Br<sub>2</sub>, Cl<sub>2</sub>, and BrCl) implies that this mechanism may be common for non-hydrogen abstraction reactions and may provide a useful tool in the prediction of reaction rate constants and mechanisms. To further examine the IP - EA trend, we have measured the rate constants for the reactions of X + ClOCl → products over the temperature range 230-400 K for X = Br, Cl, F, O, OH, and N.<sup>7</sup>



As is true for the X + ClNO and X + O<sub>3</sub> series, the similar exothermicities for the Cl abstraction in the X + ClOCl series isolates the electron delocalization effect from thermodynamic considerations.

Besides their importance in the IP - EA framework, the kinetics of ClOCl reactions with these radicals are of interest for their role as sources of ClO for atmospheric chemistry related studies. In addition, because of the similarity in structure, the reactivity of the ClO dimer (ClOOC) may be similar to the reactivity of

ClOCl. The ClO dimer has been recognized to play an important role in the destruction of ozone within regions of enhanced ClO in the antarctic vortex.<sup>8-10</sup> A knowledge of the rate constants for the reactions of ClOCl may be useful in providing an estimate of the rate constants of the ClO dimer in the arctic and the antarctic stratospheres. Also, the kinetics of HOCl, which is an important reservoir of chlorine in the stratosphere, invariably require a knowledge of the kinetics of ClOCl since HOCl samples are most easily prepared as an equilibrium mixture of H<sub>2</sub>O and ClOCl.<sup>11</sup>

These reactions are interesting from a mechanistic viewpoint because there are other thermodynamically accessible product channels besides the direct chlorine atom abstraction (for example, OH + ClOCl → HO<sub>2</sub> + Cl<sub>2</sub>, ΔH°<sub>298</sub> = -26.0 kcal/mol). A comparison of these overall rate constants with that predicted from the IP - EA trend might give some additional insight into the mechanisms of these reactions. Some of these mechanisms may involve long-lived intermediates; therefore a knowledge of the temperature and pressure dependences is crucial to the understanding of these reactions. This paper presents the rate constants and temperature dependences for reactions 1-6 using a discharge flow laser magnetic resonance (LMR)/resonance fluorescence (RF) system. This system is ideal for this type of study as it allows for simultaneous multiple detection of reactants and products. These results are then compared to those predicted by the IP - EA trend in order to test the applicability of the model.

### Experimental Section

The LMR/RF discharge-flow system used in these studies has been described elsewhere.<sup>12</sup> Briefly, the system consists of a 70-cm-length, 2.5-cm-i.d. Pyrex flow tube, surrounded by a temperature jacket for the circulation of heated or cooled fluids. A 25-cm length of 2.5-cm-i.d. Pyrex tubing connects the LMR axis to the detection axes for Br, Cl, H, and O atom RF. Retractable Pyrex tubes were used to open and close the upstream LMR and RF axes to minimize radical loss in the gap regions when the downstream RF detection axes were used. A loop injector located 5 cm upstream from the third RF axis was used for chemical conversion. All surfaces were coated with Teflon to reduce radical wall loss. Average pressure in the main reaction zone was measured using an MKS Baratron capacitance manometer.

All experiments were performed under pseudo-first-order kinetic conditions. ClOCl was added in excess through a movable 6-mm-o.d. Pyrex injector to a bulk flow of 1-4 Torr of He. ClOCl was synthesized<sup>13</sup> by condensing a 2-fold excess of Cl<sub>2</sub> at 196 K onto a dried mixture of yellow mercuric oxide and an approximately equal volume of glass beads. This mixture was allowed to react for 12 h or longer. Unreacted Cl<sub>2</sub> was removed by distillation. The resulting reddish-brown liquid was stored at 196 K. ClOCl was eluted into the reaction zone in a measured flow of ultrahigh purity (UHP) He (0.5-2 cm<sup>3</sup> (STP) s<sup>-1</sup>), and its concentration was controlled by varying the fraction of He that passed over the liquid phase. Concentrations of ClOCl were determined by UV absorption at 254 nm using a 10-cm Pyrex cell with quartz windows. The source was a Hg Pen Ray lamp, whose UV light was collected using an Ebert-Fastie monochromator (RSI 12-150) and a CsTe photomultiplier. The ClOCl fraction was calculated using Beer's law and an absorption cross section<sup>11</sup> of 1.9 × 10<sup>-18</sup> cm<sup>2</sup> and from the total pressure in the cell measured using a calibrated Ashcroft mechanical gauge.

Reagent radicals were added to the main flow either through a side arm or through a fixed injector. Radicals were detected by (1) resonance fluorescence (for Br, Cl, O, and N), (2) chemical

(2) Toohey, D. W.; Brune, W. H.; Anderson, J. G. *Int. J. Chem. Kinet.* **1988**, *20*, 131.

(3) Loewenstein, L. M.; Anderson, J. G. *J. Phys. Chem.* **1987**, *91*, 2993.

(4) Timonen, R. S.; Russell, J. J.; Sarzynski, D.; Gutman, D. *J. Phys. Chem.* **1987**, *91*, 1873.

(5) Timonen, R. S.; Gutman, D. *J. Phys. Chem.* **1986**, *90*, 2986.

(6) Paltenghi, R.; Ogryzlo, E. A.; Bayes, K. D. *J. Phys. Chem.* **1984**, *88*, 2595.

(7) Thermochemical quantities are from: JANAF Thermochemical Tables, 3rd ed.; Chase, M. W., Jr., Davies, C. A., Downey, J. A., Jr., Fruip, P. J., McDonald, R. A., Syverud, A. N., Eds.; *J. Phys. Chem. Ref. Data, Suppl. 1* **1985**, *14*. ΔH<sub>f</sub> for ClN assumed to be approximately 75 kcal/mol from the ab initio calculations of: Bettendorff, M.; Peyrimhoff, S. D. *Chem. Phys.* **1986**, *104*, 29.

(8) Molina, L. T.; Molina, M. J. *J. Phys. Chem.* **1987**, *91*, 433.

(9) Anderson, J. G.; Brune, W. H.; Lloyd, S. A.; Toohey, D. W.; Sander, S. P.; Starr, W. L.; Loewenstein, M.; Podolske, J. R. *J. Geophys. Res.* **1989**, *94*, 11465.

(10) Anderson, J. G.; Toohey, D. W.; Brune, W. H. *Science* **1991**, *251*, 39.

(11) Molina, L. T.; Molina, M. J. *J. Phys. Chem.* **1978**, *82*, 2410.

(12) Brune, W. H.; Schwab, J. J.; Anderson, J. G. *J. Phys. Chem.* **1983**, *87*, 4503.

(13) Schack, C. J.; Lindahl, C. B. *Inorg. Nucl. Chem. Lett.* **1967**, *3*, 387.

TABLE I: Br + ClOCl → BrCl + ClO Summary of Experimental Conditions

reported rate constant $k_1$	$(2.1 \pm 0.2) \times 10^{-11} \exp[(-435 \pm 30)/T] \text{ cm}^3 \text{ molecule}^{-1} \text{ s}^{-1}$ for 233 K $\leq T \leq$ 402 K
no. of experiments	$k_1, \text{ cm}^3 \text{ molecule}^{-1} \text{ s}^{-1}$
39 at 298 K	$(4.8 \pm 0.2) \times 10^{-12}$
8 at 402 K	$(7.1 \pm 0.2) \times 10^{-12}$
9 at 373 K	$(6.5 \pm 0.2) \times 10^{-12}$
8 at 341 K	$(5.8 \pm 0.1) \times 10^{-12}$
6 at 316 K	$(5.1 \pm 0.2) \times 10^{-12}$
7 at 266 K	$(3.9 \pm 0.2) \times 10^{-12}$
7 at 244 K	$(3.6 \pm 0.2) \times 10^{-12}$
6 at 233 K	$(3.4 \pm 0.3) \times 10^{-12}$
pressure range	1.1–2.1 Torr
flow velocity range	8.1–13.3 m s <sup>-1</sup>
carrier gas	He
diffusion coefficient	Br–He, $0.087T^{3/2}/P$ (<3% correction)
species detected	Br (RF)
excess reactant	ClOCl = $(0.08\text{--}4.1) \times 10^{13} \text{ molecules cm}^{-3}$
initial Br concentration	$(0.2\text{--}1.4) \times 10^{11} \text{ cm}^{-3}$
stoichiometric ratio	10–300
observed first-order injector wall removal rates	<4 s <sup>-1</sup>

conversion followed by resonance fluorescence (for F and ClO), and (3) laser magnetic resonance (for OH and HO<sub>2</sub>).

**Radical Sources and Detection.** For the measurement of reaction 1, Br atoms were produced by the chemical titration of Cl with excess Br<sub>2</sub>, via the fast reaction Cl + Br<sub>2</sub> → Br + BrCl. Cl atoms were produced by a microwave discharge of trace Cl<sub>2</sub> in UHP He using a phosphoric acid-coated tube. Br<sub>2</sub> was added downstream through a 1/16-in.-o.d. Teflon tube inserted inside a 22-cm-length, 6-mm-o.d. Pyrex injector coated with Teflon. This injector entered the main reactor through a side-arm inlet. The resonance fluorescence detection of Br employed a sealed light source and collection optics described elsewhere.<sup>14</sup> The sensitivity to Br atoms was typically  $5 \times 10^{-7}$  counts s<sup>-1</sup>/(atom cm<sup>-3</sup>) with background signals of <200 counts s<sup>-1</sup>, resulting in a detection limit of <1 × 10<sup>7</sup> atoms cm<sup>-3</sup> at S/N = 1 for 10-s integration periods.

For the rate measurement of reaction 2, Cl atoms were produced as above using a microwave discharge of trace Cl<sub>2</sub>. The sealed light source employed for Cl resonance fluorescence detection has also been described in detail elsewhere.<sup>15</sup> Sensitivity to Cl atoms was typically  $3 \times 10^{-8}$  counts s<sup>-1</sup>/(atom cm<sup>-3</sup>) with background signals of <20 counts s<sup>-1</sup> resulting in a detection limit of <5 × 10<sup>7</sup> atoms cm<sup>-3</sup> at S/N = 1 for 10-s integrations using the F + Cl<sub>2</sub> → ClF + Cl reaction for calibration.

The F atoms used in the measurement of reaction 3 were produced by a microwave discharge of either trace F<sub>2</sub> or CF<sub>4</sub> in UHP He in an alumina tube. F atoms were added to the main reactor through a 6-mm-o.d., 180-cm-length Pyrex injector, coated with Teflon, whose position was held fixed upstream of the main reacting region. Addition of F through the long injector helped to reduce H atom impurities associated with the production of fluorine radicals.<sup>16</sup> F atoms were detected by chemical conversion to H using the fast F + H<sub>2</sub> → HF + H reaction, and the resulting H atoms were detected by RF. H<sub>2</sub> was added in the loop injector upstream of the third detection axis. The light source was a combination H and O sealed lamp similar to that described in detail elsewhere.<sup>12</sup> To isolate the hydrogen Ly-α line at 121.6 nm, O<sub>2</sub> was flowed through a 2-mm filter between the lamp and the optical baffles to absorb the oxygen triplet at 130.4 nm. The sensitivity of this lamp to H atoms was typically  $9 \times 10^{-7}$  counts s<sup>-1</sup>/(atom cm<sup>-3</sup>) with a scattered-light count of <200 counts s<sup>-1</sup>, resulting in a detection limit of <7 × 10<sup>6</sup> atoms cm<sup>-3</sup> at S/N = 1 and 10-s integration periods.

For the measurement of the rate of reaction 4, O atoms were produced in a side arm using a microwave discharge of O<sub>2</sub> in UHP He in an uncoated quartz tube. The radicals were detected using

the H/O lamp described above. To isolate the O atom emissions, a CaF<sub>2</sub> filter and a purge of N<sub>2</sub> were used to eliminate the hydrogen Ly-α emission. The sensitivity of this lamp to O atoms was  $1 \times 10^{-8}$  counts s<sup>-1</sup>/(atom cm<sup>-3</sup>) with background signals of typically <200 counts s<sup>-1</sup>, giving a detection limit of <5 × 10<sup>8</sup> atoms cm<sup>-3</sup> (S/N = 1, 10-s integration).

OH radicals used in reaction 5 were made using the titration reaction F + H<sub>2</sub>O → HF + OH. F atoms were produced as above, and an H<sub>2</sub>O/UHP He mixture was added through a 1/16-in.-o.d. Teflon tube inserted inside the 180-cm length injector. The H<sub>2</sub>O/He mixture was produced by bubbling He sequentially through two traps containing distilled H<sub>2</sub>O. OH was also produced using the H + NO<sub>2</sub> → OH + NO reaction by discharging H<sub>2</sub> in an uncoated quartz tube and adding NO<sub>2</sub> through the 1/16-in. Teflon line inserted in a side-arm injector. For both sources, the injector was held fixed upstream of the reaction zone. OH radicals were detected by laser magnetic resonance at 3.8 kG using the σ-polarized 163-μm CH<sub>3</sub>OH laser line pumped by the 10R(38) CO<sub>2</sub> laser emission. The sensitivity to OH was typically  $2 \times 10^7$  atom cm<sup>-3</sup> at S/N = 1 and a 1-s time constant, calibrated as before.<sup>12</sup>

For the rate measurement of reaction 6, N atoms were produced by microwave discharge of UHP N<sub>2</sub> in UHP He and added to the main reactor through a side arm or through the 180-cm-length injector. Addition of N through the long injector reduced H and O impurities. N atoms were detected by resonance fluorescence using a flowing N<sub>2</sub> light source. The 120.0-nm <sup>4</sup>P–<sup>4</sup>S° (3s–2p) emission of N was isolated from emissions by O impurities in the lamp by flowing CO<sub>2</sub> through the 2-mm filter. This eliminated the O emission at 130.2 nm but passed radiation from H impurities at 121.6 nm into the detection volume. Hydrogen impurities in the source discharge (<3 × 10<sup>8</sup> cm<sup>-3</sup>) were detected simultaneously using the H lamp described above. This ensured that the observed fluorescence from the N lamp axis was due solely to nitrogen atoms. The sensitivity to N was typically  $2 \times 10^{-7}$  counts s<sup>-1</sup>/(atom cm<sup>-3</sup>) with backgrounds <70 counts s<sup>-1</sup>, resulting in a detection limit of <1 × 10<sup>7</sup> cm<sup>-3</sup> at S/N = 1 and 10-s integration periods.

The following laboratory gases were used with their stated purities: He (HP, 99.99%) for bulk flow, He (UHP 99.999%) for all discharges and mixtures, CF<sub>4</sub> (99.7%), Cl<sub>2</sub> (HP, 99.5%), F<sub>2</sub> (2% mixture, UHP He balance), H<sub>2</sub> (UHP, 99.999%), O<sub>2</sub> (UHP, 99.99%), N<sub>2</sub> (UHP, 99.99%), NO (CP, 99.0%), and NO<sub>2</sub> (99.5%). All gases were supplied by Matheson except the HP and UHP He and the UHP N<sub>2</sub> which were supplied by Northeast Airgas. NO and Br<sub>2</sub> (J. T. Baker Chemical Co., >99.8%) were purified as described previously.<sup>2,14</sup>

## Experimental Results

The experimental conditions for reactions 1–6 are summarized in Tables I–VI. The first-order decay rates ( $k_{\text{obsd}}^1$ ) were obtained from a weighted linear least-squares fit of the logarithm of the

(14) Toohey, D. W.; Brune, W. H.; Anderson, J. G. *J. Phys. Chem.* **1987**, *91*, 1215.

(15) Schwab, J. J.; Anderson, J. G. *J. Quant. Spectrosc. Radiat. Transfer* **1982**, *21*, 445.

(16) Stevens, P. S.; Brune, W. H.; Anderson, J. G. *J. Phys. Chem.* **1989**, *93*, 4068.

TABLE II: Cl + ClOCl → Cl<sub>2</sub> + ClO Summary of Experimental Conditions

reported rate constant $k_2$	$(6.0 \pm 0.6) \times 10^{-11} \exp[(127 \pm 30)/T] \text{ cm}^3 \text{ molecule}^{-1} \text{ s}^{-1}$ for $233 \text{ K} \leq T \leq 373 \text{ K}$
no. of experiments	$k_2, \text{ cm}^3 \text{ molecule}^{-1} \text{ s}^{-1}$
27 at 298 K	$(9.1 \pm 0.4) \times 10^{-11}$
7 at 373 K	$(8.3 \pm 0.6) \times 10^{-11}$
6 at 353 K	$(8.2 \pm 0.6) \times 10^{-11}$
7 at 325 K	$(8.8 \pm 0.4) \times 10^{-11}$
9 at 265 K	$(1.00 \pm 0.06) \times 10^{-10}$
6 at 233 K	$(1.02 \pm 0.04) \times 10^{-10}$
pressure range	1.0–2.0 Torr
flow velocity range	8.2–12.3 m s <sup>-1</sup>
carrier gas	He
diffusion coefficient	Cl–He, $0.104T^{3/2}/P$ (<3% correction)
species detected	Cl (RF)
excess reactant	ClOCl = $(0.08\text{--}3.2) \times 10^{12} \text{ molecules cm}^{-3}$
initial Cl concentration	$(0.4\text{--}2.1) \times 10^{11} \text{ cm}^{-3}$
stoichiometric ratio	2–40
observed first-order injector wall removal rates	<4 s <sup>-1</sup>

TABLE III: F + ClOCl → ClF + ClO Summary of Experimental Conditions

reported rate constant $k_3$	$(1.5 \pm 0.5) \times 10^{-10} \exp[(-47 \pm 94)/T] \text{ cm}^3 \text{ molecule}^{-1} \text{ s}^{-1}$ for $263 \text{ K} \leq T \leq 373 \text{ K}$
no. of experiments	$k_3, \text{ cm}^3 \text{ molecule}^{-1} \text{ s}^{-1}$
23 at 298 K	$(1.3 \pm 0.3) \times 10^{-10}$
6 at 373 K	$(1.3 \pm 0.2) \times 10^{-10}$
7 at 348 K	$(1.3 \pm 0.2) \times 10^{-10}$
8 at 325 K	$(1.4 \pm 0.2) \times 10^{-10}$
6 at 273 K	$(1.3 \pm 0.4) \times 10^{-10}$
6 at 263 K	$(1.2 \pm 0.2) \times 10^{-10}$
pressure range	1.2–2.0 Torr
flow velocity range	8.7–12.1 m s <sup>-1</sup>
carrier gas	He
diffusion coefficient	F–He, $0.153T^{3/2}/P$ (<3% correction)
species detected	F (chemical conversion to H) H (RF)
excess reactant	ClOCl = $(0.02\text{--}1.4) \times 10^{12} \text{ molecules cm}^{-3}$
initial F concentration	$(0.3\text{--}1.3) \times 10^{10} \text{ cm}^{-3}$
stoichiometric ratio	7–250
observed first-order injector wall removal rates	<2 s <sup>-1</sup>

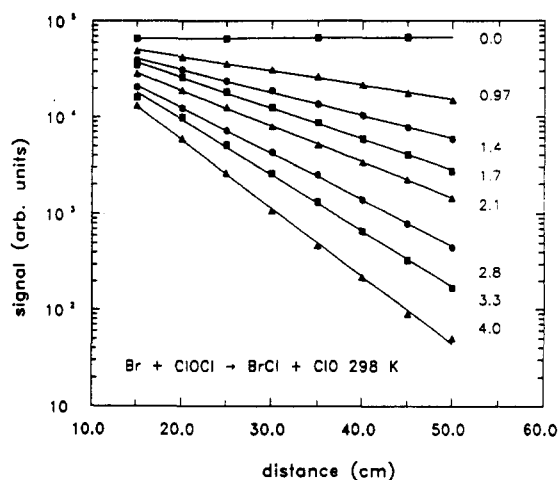


Figure 1. Series of typical decay plots of radical signal versus injector distance (for reaction 1, 298 K). Values for ClOCl concentrations are in  $10^{13} \text{ molecules cm}^{-3}$ .

detected radical signal versus injector distance ( $k_{\text{decay}}^I$ ) and corrected for axial diffusion and probe loss by<sup>17</sup>

$$k_{\text{obsd}}^I = k_{\text{decay}}^I (1 + k_{\text{decay}}^I D / \bar{v}^2) - k_{\text{probe}}$$

where  $\bar{v}$  is the mean bulk flow velocity,  $D$  is the radical diffusion coefficient, and  $k_{\text{probe}}$  is the first-order radical loss rate on the movable injector. Bimolecular rate constants ( $k$ ) were calculated from a linear least-squares fit of the plots of  $k_{\text{obsd}}^I$  versus excess reagent concentration.

**Br + ClOCl → BrCl + ClO.** Table I summarizes the experimental results for reaction 1. A series of typical decay plots for

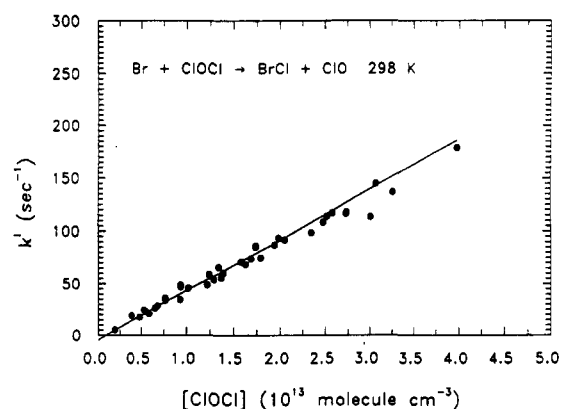


Figure 2. Plot of  $k_{\text{obsd}}^I$  vs ClOCl concentration for  $\text{Br} + \text{ClOCl} \rightarrow \text{BrCl} + \text{ClO}$  at room temperature.

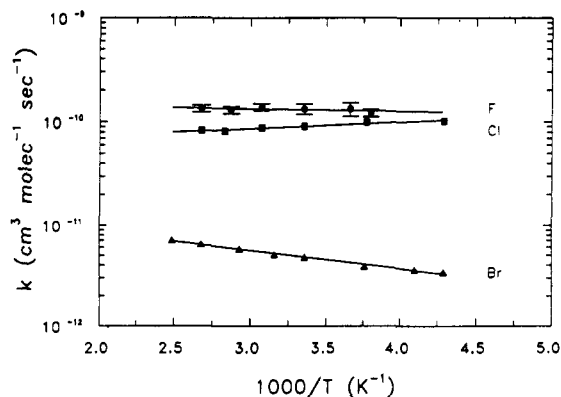


Figure 3. Semilogarithmic plot of  $k$  vs  $1/T$  for reactions 1–3. Error is  $1\sigma$ . Omitted error bars indicate the uncertainty is smaller than the size of the symbol.

**TABLE IV: O + ClOCl → ClO + ClO Summary of Experimental Conditions**

reported rate constant $k_4$	$(2.7 \pm 0.2) \times 10^{-11} \exp[(-510 \pm 30)/T] \text{ cm}^3 \text{ molecule}^{-1} \text{ s}^{-1}$ for $230 \text{ K} \leq T \leq 380 \text{ K}$
no. of experiments	$k_4, \text{ cm}^3 \text{ molecule}^{-1} \text{ s}^{-1}$
25 at 298 K	$(4.7 \pm 0.2) \times 10^{-12}$
9 at 380 K	$(7.1 \pm 0.2) \times 10^{-12}$
9 at 353 K	$(6.4 \pm 0.3) \times 10^{-12}$
9 at 340 K	$(6.0 \pm 0.4) \times 10^{-12}$
8 at 318 K	$(5.5 \pm 0.4) \times 10^{-12}$
12 at 266 K	$(4.2 \pm 0.3) \times 10^{-12}$
11 at 246 K	$(3.4 \pm 0.2) \times 10^{-12}$
7 at 230 K	$(2.9 \pm 0.2) \times 10^{-12}$
pressure range	1.9–2.1 Torr
flow velocity range	8.0–13.0 m s <sup>-1</sup>
carrier gas	He
diffusion coefficient	O–He, $0.135T^{3/2}/P$ (<3% correction)
species detected	O (RF)
excess reactant	ClOCl = $(0.08\text{--}4.2) \times 10^{13} \text{ molecules cm}^{-3}$
initial O concentration	$(2.5\text{--}6.0) \times 10^{11} \text{ cm}^{-3}$
stoichiometric ratio	2–80
observed first-order injector wall removal rates	<2 s <sup>-1</sup>

**TABLE V: OH + ClOCl → Products Summary of Experimental Conditions**

reported rate constant $k_5$	$(1.7 \pm 0.8) \times 10^{-12} \exp[(420 \pm 170)/T] \text{ cm}^3 \text{ molecule}^{-1} \text{ s}^{-1}$ for $236 \text{ K} \leq T \leq 383 \text{ K}$
no. of experiments	$k_5, \text{ cm}^3 \text{ molecule}^{-1} \text{ s}^{-1}$
24 at 298 K	$(7.4 \pm 0.6) \times 10^{-12}$
7 at 383 K	$(5.1 \pm 1.0) \times 10^{-12}$
7 at 358 K	$(5.0 \pm 1.2) \times 10^{-12}$
13 at 338 K	$(5.2 \pm 0.8) \times 10^{-12}$
8 at 273 K	$(8.4 \pm 0.7) \times 10^{-12}$
6 at 254 K	$(8.4 \pm 1.0) \times 10^{-12}$
11 at 236 K	$(8.8 \pm 1.5) \times 10^{-12}$
pressure range	1.1–3.9 Torr
	$k_{1 \text{ Torr}} = (6.5 \pm 0.8) \times 10^{-12} \text{ cm}^3 \text{ molecule}^{-1} \text{ s}^{-1}$
	$k_{2 \text{ Torr}} = (7.4 \pm 0.6) \times 10^{-12} \text{ cm}^3 \text{ molecule}^{-1} \text{ s}^{-1}$
	$k_{4 \text{ Torr}} = (8.1 \pm 0.4) \times 10^{-12} \text{ cm}^3 \text{ molecule}^{-1} \text{ s}^{-1}$
flow velocity range	7.6–11.5 m s <sup>-1</sup>
carrier gas	He
diffusion coefficient	OH–He, $0.145T^{3/2}/P$ (<5% correction)
species detected	OH (LMR) HO <sub>2</sub> (LMR) ClO (conversion to Cl) Cl (RF)
excess reactant	ClOCl = $(0.24\text{--}3.3) \times 10^{13} \text{ molecules cm}^{-3}$
initial OH concentration	$(0.1\text{--}1.3) \times 10^{11} \text{ cm}^{-3}$
stoichiometric ratio	48–660
observed first-order injector wall removal rates	<10 s <sup>-1</sup>

**TABLE VI: N + ClOCl → Products Summary of Experimental Conditions**

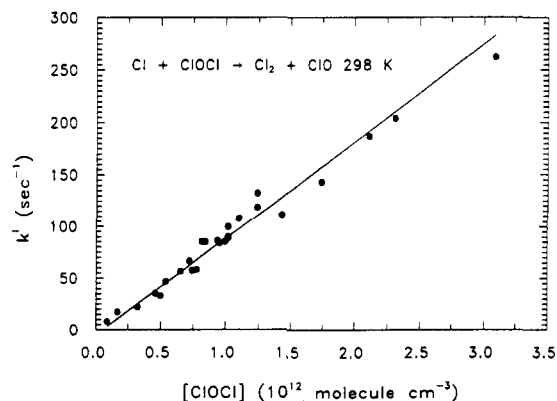
reported rate constant	$k_6^{298} < 6 \times 10^{-15} \text{ cm}^3 \text{ molecule}^{-1} \text{ s}^{-1}$ $k_6^{373} < 3 \times 10^{-15} \text{ cm}^3 \text{ molecule}^{-1} \text{ s}^{-1}$
pressure range	2.3–2.5 Torr
flow velocity range	10.0–12.4 m s <sup>-1</sup>
carrier gas	He
species detected	N (RF)
excess reactant	ClOCl < $2.5 \times 10^{14} \text{ molecules cm}^{-3}$
initial N concentration	< $2 \times 10^{11} \text{ cm}^{-3}$
observed first-order injector wall removal rates	<2 s <sup>-1</sup>

this reaction is shown in Figure 1 and are representative of the quality of data for all reactions reported here. These decays were linear over a factor of 100 after a background signal due to Br<sub>2</sub> photolysis was subtracted from the observed signal. The plot of  $k_{\text{obsd}}^1$  versus ClOCl concentration for the data at room temperature appears in Figure 2. A weighted least-squares fit of the data yields a value of

$$k_1^{298} = (4.8 \pm 0.2) \times 10^{-12} \text{ cm}^3 \text{ molecule}^{-1} \text{ s}^{-1}$$

for the rate constant at room temperature. The reported error is 2σ from the precision of the least-squares analysis. The measurements at various temperatures yield the Arrhenius plot shown in Figure 3, and a least-squares analysis gives

$$k_1 = (2.1 \pm 0.2) \times 10^{-11} \exp[(-435 \pm 30)/T] \text{ cm}^3 \text{ molecule}^{-1} \text{ s}^{-1}$$

**Figure 4.** Plot of  $k_{\text{obsd}}^1$  vs ClOCl concentration for Cl + ClOCl → Cl<sub>2</sub> + ClO at room temperature.

over the temperature range 233–402 K. This result is in good agreement with that reported by Sander and Friedl<sup>18</sup> using flash photolysis/UV spectrometry. They found  $k_1 = (2.14 \pm 0.89) \times 10^{-11} \exp[(-520 \pm 130)/T] \text{ cm}^3 \text{ molecule}^{-1} \text{ s}^{-1}$  over the temperature range 220–298 K.

Cl + ClOCl → Cl<sub>2</sub> + ClO. Table II summarizes the results and experimental parameters for reaction 2. Decays of the logarithm of the Cl atom signal were linear over a factor of 100 after

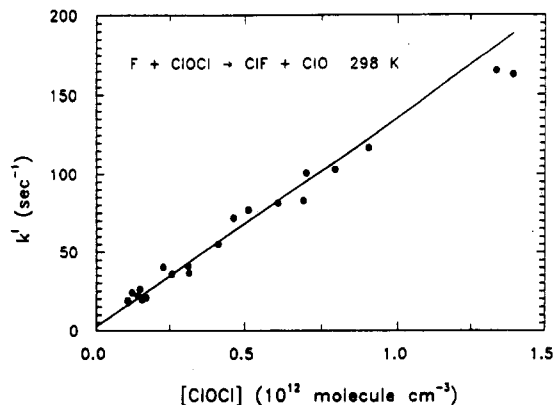


Figure 5. Plot of  $k_{\text{obs}}^1$  vs ClOCl concentration for  $\text{F} + \text{ClOCl} \rightarrow \text{ClF} + \text{ClO}$  at room temperature.

subtraction of the scattered-light signal. Figure 4 shows the room-temperature pseudo-first-order plot of  $k_{\text{obs}}^1$  versus ClOCl concentration, and the rate constants at various temperatures are shown in Figure 3. A least-squares analysis of the results gives

$$k_2^{298} = (9.1 \pm 0.4) \times 10^{-11} \text{ cm}^3 \text{ molecule}^{-1} \text{ s}^{-1}$$

$$k_2 = (6.0 \pm 0.6) \times 10^{-11} \exp[(127 \pm 30)/T] \text{ cm}^3 \text{ molecule}^{-1} \text{ s}^{-1}$$

over the temperature range 233–373 K.

The room-temperature value reported here is in excellent agreement with the rate constant reported by Ray et al.<sup>19</sup> using a discharge flow system and employing resonance fluorescence and mass spectrometric detection techniques. They reported an unweighted average of  $k_2^{298} = (9.8 \pm 0.8) \times 10^{-11} \text{ cm}^3 \text{ molecule}^{-1} \text{ s}^{-1}$  for the two measurements. No temperature studies were reported. The result reported here is also in good agreement with the results of Burrows and Cox,<sup>20</sup> who measured the room-temperature rate of reaction 2 using modulated flash photolysis. They found  $k_2^{298} = (1.0 \pm 0.35) \times 10^{-10} \text{ cm}^3 \text{ molecule}^{-1} \text{ s}^{-1}$ .

$\text{F} + \text{ClOCl} \rightarrow \text{ClF} + \text{ClO}$ . The experimental parameters and results for reaction 3 are summarized in Table III. After subtracting the background signal due to H atom impurities produced in the discharge ( $<3 \times 10^8 \text{ cm}^{-3}$ ), converted fluorine decays were linear over a factor of 100. A plot of  $k_{\text{obs}}^1$  versus ClOCl concentration for the data at 298 K appears in Figure 5. The slope of this line yields

$$k_3^{298} = (1.4 \pm 0.4) \times 10^{-10} \text{ cm}^3 \text{ molecule}^{-1} \text{ s}^{-1}$$

for the rate constant at room temperature. No significant temperature dependence was measured over the temperature range studied, as can be seen from the Arrhenius plot in Figure 3. A weighted least-squares fit of the data results in a reported value of

$$k_3 = (1.5 \pm 0.5) \times 10^{-10} \exp[(-47 \pm 94)/T] \text{ cm}^3 \text{ molecule}^{-1} \text{ s}^{-1}$$

over the temperature range 263–373 K. This is the first published measurement for the rate of this reaction.

$\text{O} + \text{ClOCl} \rightarrow \text{ClO} + \text{ClO}$ . Table IV summarizes the experimental parameters for reaction 4. Radical decays were linear over a factor of 2–100 after subtraction of a background signal ( $<500 \text{ counts s}^{-1}$ ) which was probably due to ClOCl photolysis forming an O atom and  $\text{Cl}_2$ . This background was measured after each experiment and increased with increasing concentrations of ClOCl. The experiments at room temperature are shown plotted in Figure 6, and the measurements at various temperatures result

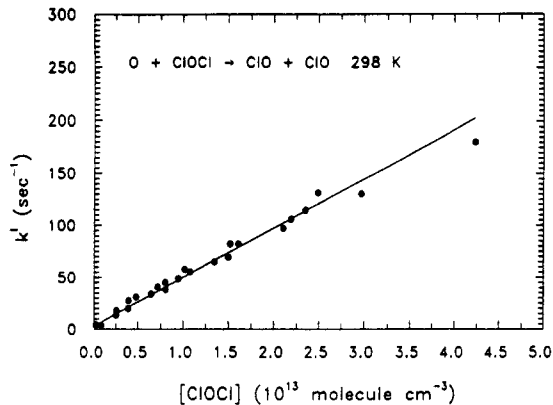


Figure 6. Plot of  $k_{\text{obs}}^1$  vs ClOCl concentration for  $\text{O} + \text{ClOCl} \rightarrow \text{ClO} + \text{ClO}$  at room temperature.

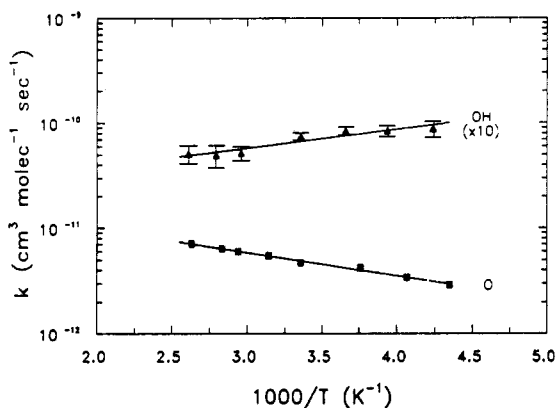


Figure 7. Semilogarithmic plot of  $k$  vs  $1/T$  for reactions 4 and 5. Error is  $2\sigma$ . Omitted error bars indicate the uncertainty is smaller than the size of the symbol. The rate constants for the  $\text{OH} + \text{ClOCl}$  reaction have been multiplied by 10 for clarity.

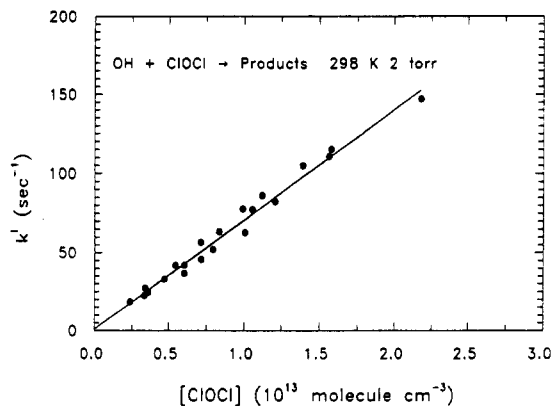


Figure 8. Plot of  $k_{\text{obs}}^1$  vs ClOCl concentration for  $\text{OH} + \text{ClOCl} \rightarrow \text{HOCl} + \text{ClO}$  at room temperature.

in the Arrhenius plot shown in Figure 7. A weighted least-squares analysis of this data gives

$$k_4^{298} = (4.7 \pm 0.2) \times 10^{-12} \text{ cm}^3 \text{ molecule}^{-1} \text{ s}^{-1}$$

$$k_4 = (2.7 \pm 0.2) \times 10^{-11} \exp[(-513 \pm 30)/T] \text{ cm}^3 \text{ molecule}^{-1} \text{ s}^{-1}$$

over the temperature range 230–380 K.

Both the room-temperature rate constant and the temperature dependence reported here are in excellent agreement with the values reported by Miziolek and Molina<sup>21</sup> using a discharge-flow system. In their study, oxygen atoms were converted to  $\text{NO}_2$ , and the resulting product chemiluminescence was detected. They found  $k_4 = (2.7 \pm 0.3) \times 10^{-11} \exp[(-560 \pm 80)/T] \text{ cm}^3 \text{ mole-}$

(19) Ray, G. W.; Keyser, L. F.; Watson, R. T. *J. Phys. Chem.* **1980**, *84*, 1674.

(20) Burrows, J. P.; Cox, R. A. *J. Chem. Soc., Faraday Trans. 1* **1981**, *77*, 2465.

(21) Miziolek, A. W.; Molina, M. J. *J. Phys. Chem.* **1978**, *82*, 1769.

cule<sup>-1</sup> s<sup>-1</sup> and a room-temperature value of  $(4.1 \pm 0.5) \times 10^{-12}$  cm<sup>3</sup> molecule<sup>-1</sup> s<sup>-1</sup>. The room-temperature result of Freeman and Phillips<sup>22</sup> using a discharge-flow/mass spectrometric technique is not in good agreement with the data reported here. They found  $k_4^{298} = (1.4 \pm 0.2) \times 10^{-11}$  cm<sup>3</sup> molecule<sup>-1</sup> s<sup>-1</sup>. This experiment was performed in excess oxygen atoms, and the rate constant was calculated indirectly by an attempt to model the secondary chemistry in their system. This is a difficult experiment because it requires an accurate knowledge of a number of different rate constants.

**OH + ClOCl → Products.** Table V summarizes the experimental conditions for the measurement of reaction 5. OH decays were linear over a factor of 2–60. Figure 8 shows the results at room temperature, and a weighted least-squares fit of the data yields a value of

$$k_5^{298} = (7.4 \pm 0.6) \times 10^{-12} \text{ cm}^3 \text{ molecule}^{-1} \text{ s}^{-1}$$

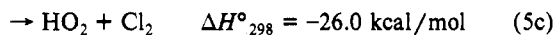
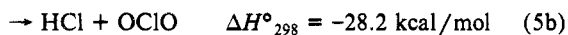
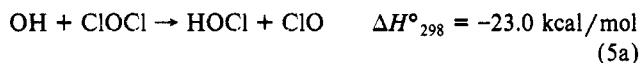
for the rate constant at 2-Torr total pressure. The measurements at various temperatures and 2 Torr are shown in Figure 7, and the slope of this line gives

$$k_5 = (1.7 \pm 0.8) \times 10^{-12} \exp[(420 \pm 170)/T] \text{ cm}^3 \text{ molecule}^{-1} \text{ s}^{-1}$$

over the temperature range 236–383 K. The room-temperature result reported above for this reaction is in fair agreement with a preliminary investigation reported by Ennis and Birks<sup>23</sup> in conjunction with their study of the OH + HOCl reaction. They found  $k_5^{298} = (9.4 \pm 1.0) \times 10^{-12}$  cm<sup>3</sup> molecule<sup>-1</sup> s<sup>-1</sup> using a discharge-flow system and resonance fluorescence detection of OH. The room-temperature value reported here is in better agreement with the result of Leu and Lin,<sup>24</sup> who found  $k_5^{298} = (6.5 \pm 0.5) \times 10^{-12}$  cm<sup>3</sup> molecule<sup>-1</sup> s<sup>-1</sup> using a discharge-flow/resonance fluorescence system. The temperature dependence for this reaction has not been previously reported.

The negative temperature dependence for this reaction suggests a possible complex mechanism involving a long-lived intermediate (see Discussion section below). At high temperatures, the pseudo-first-order decays showed significant curvature at long reaction times that was independent of the initial OH concentration. For this reason, the uncertainty for the rate constants at higher temperatures is unusually large. A long-lived intermediate would account for the observed decay curvature, as at high temperatures, steady-state re-formation of reactants would be favored at long reaction times.

The OH + ClOCl reaction has three thermodynamically accessible product channels:



The ClO and HO<sub>2</sub> product yields for this reaction were monitored in order to determine the relative importance of the three channels for this reaction. ClO was detected by chemical conversion to Cl using the fast ClO + NO reaction, and the resulting Cl atoms were detected using resonance fluorescence while simultaneously the OH reactant concentration was measured with the LMR spectrometer. Approximately 10<sup>14</sup> cm<sup>-3</sup> of NO was added through the loop injector upstream of the third RF axis. LMR detection of HO<sub>2</sub> employed the same laser line as OH, but at a magnetic field of 2.3 kG.

At room temperature, no HO<sub>2</sub> was observed, placing an upper limit on the rate constant for this channel of  $k_{5c}^{298} < 1 \times 10^{-14}$  cm<sup>3</sup> molecule<sup>-1</sup> s<sup>-1</sup>, based on a typical reaction time of 50 ms. Because of the low concentrations of OH present in the system ( $< 5 \times 10^{10}$

cm<sup>-3</sup>), loss of HO<sub>2</sub> from reaction with OH ( $k^{298} = 1 \times 10^{-10}$  cm<sup>3</sup> molecule<sup>-1</sup> s<sup>-1</sup>) would have been insignificant. A high yield of ClO was observed as a product of reaction 5. But because of uncertainties involving the chemistry of the system, it is difficult to determine a branching ratio based solely on the observed ClO production. The reaction of the converted Cl with ClOCl was not a problem because another ClO molecule was produced in the reaction; however, OCIO produced from reaction 5b would be partially converted to ClO from the NO + OCIO → NO<sub>2</sub> + ClO reaction ( $k^{298} = 3.4 \times 10^{-13}$  cm<sup>3</sup> molecule<sup>-1</sup> s<sup>-1</sup>). This would result in an overestimation of the ClO yield from reaction 5a. To measure the branching ratio for this reaction, future experiments will involve detecting ClO directly using LMR while measuring OH using RF, thus distinguishing between reactions 5a and 5b.

The OH + ClOCl reaction also exhibits a strong pressure dependence, further suggesting the existence of a long-lived intermediate. The rate constant for this reaction was measured at 1, 2, and 4 Torr, and the rate constants at the different pressures are

$$k_{1\text{Torr}}^{298} = (6.5 \pm 0.8) \times 10^{-12} \text{ cm}^3 \text{ molecule}^{-1} \text{ s}^{-1}$$

$$k_{2\text{Torr}}^{298} = (7.4 \pm 0.6) \times 10^{-12} \text{ cm}^3 \text{ molecule}^{-1} \text{ s}^{-1}$$

$$k_{4\text{Torr}}^{298} = (8.1 \pm 0.4) \times 10^{-12} \text{ cm}^3 \text{ molecule}^{-1} \text{ s}^{-1}$$

A high yield of ClO was also detected at 4 Torr using the chemical conversion technique, suggesting that the formation of the bimolecular products is still favorable at room temperature and the higher pressure.

**N + ClOCl → Products.** Table VI summarizes the experimental result and conditions for the measurement of reaction 6. No significant decay of the N signal was observed for the highest concentrations of ClOCl produced. From a least-squares fit of the observed signal at the maximum concentration of ClOCl added to the system, an upper limit of

$$k_6^{298} < 6 \times 10^{-15} \text{ cm}^3 \text{ molecule}^{-1} \text{ s}^{-1}$$

is reported for the room-temperature rate constant. Similarly, no observed decay was observed for this reaction at temperatures as high as 373 K, resulting in an upper limit of  $k_6^{373} < 3 \times 10^{-15}$  cm<sup>3</sup> molecule<sup>-1</sup> s<sup>-1</sup>. These results do not agree with those reported by Freeman and Phillips,<sup>25</sup> who found a much larger rate constant for this reaction using a mass spectrometer in a fast-flow system. They report a room-temperature rate constant of  $(1.5 \pm 0.3) \times 10^{-12}$  cm<sup>3</sup> molecule<sup>-1</sup> s<sup>-1</sup> by following decays of ClOCl in a large excess of N and modeling the secondary chemistry of the system to determine the rate of the primary reaction. Again, this is a difficult experiment because a number of rate constants for the secondary chemistry assumed to be present in their system (N + NCl → N<sub>2</sub> + Cl, N + ClO → NCl + O) remain unknown. They also found no evidence of NCl production, which they assumed to be a primary product, attributing this observation to wall loss in their ionization chamber or interaction with the sampling leak.

## Discussion

Table VII summarizes the experimental results, and the electronic and thermodynamic properties for the Cl abstraction channels for reactions 1–6. The experimental value for the ionization potential for ClOCl is 11.02 eV,<sup>26</sup> which is less than the IP of each radical in the series. On the basis of the IP – EA model, the direction of electron delocalization will be from ClOCl (lower IP) to X, and the reactivity of each system will increase as the value of IP(ClOCl) – EA(X) decreases.

The IP – EA trend for the room-temperature reactions of X + ClNO,<sup>1</sup> O<sub>3</sub>,<sup>2</sup> Cl<sub>2</sub>,<sup>3</sup> and ClOCl appears in Figure 9. In this figure, the dashed line is a fit to all the reactions of ClNO, O<sub>3</sub>, and Cl<sub>2</sub>, while the solid line is a linear fit to the data excluding

(22) Freeman, C. G.; Phillips, L. F. *J. Phys. Chem.* **1968**, *72*, 3025.

(23) Ennis, C. A.; Birks, J. W. *J. Phys. Chem.* **1988**, *92*, 1119.

(24) Leu, M. T.; Lin, C. L. *Geophys. Res. Lett.* **1979**, *6*, 425.

(25) Freeman, C. G.; Phillips, L. F. *J. Phys. Chem.* **1968**, *72*, 3028.

(26) Cornford, A. B.; Frost, D. C.; Herring, F. G.; McDowell, C. A. *J. Chem. Phys.* **1971**, *55*, 2820.

TABLE VII: X + ClOCl → XCl + ClO Electronic Properties and Summary of Experimental Results

radical	EA, <sup>a</sup> eV	IP, <sup>a</sup> eV	experimental value			
			A factor, cm <sup>3</sup> molec <sup>-1</sup> s <sup>-1</sup>	E <sub>a</sub> , kcal/mol	k <sup>298</sup> , cm <sup>3</sup> molec <sup>-1</sup> s <sup>-1</sup>	ΔH <sub>298</sub> , kcal/mol
Cl	3.62	13.0	(6.0 ± 0.6) × 10 <sup>-11</sup>	-0.25 ± 0.06	(9.1 ± 0.4) × 10 <sup>-11</sup>	-24.0
F	3.45	17.4	(1.5 ± 0.5) × 10 <sup>-10</sup>	0.09 ± 0.18	(1.3 ± 0.3) × 10 <sup>-10</sup>	-26.2
Br	3.37	11.8	(2.1 ± 0.2) × 10 <sup>-11</sup>	0.86 ± 0.06	(4.8 ± 0.2) × 10 <sup>-12</sup>	-18.3
OH	1.9	13.2	(1.7 ± 0.8) × 10 <sup>-12</sup>	-0.83 ± 0.34	(7.4 ± 0.6) × 10 <sup>-12</sup>	-23.0
O	1.46	13.6	(2.7 ± 0.2) × 10 <sup>-11</sup>	1.01 ± 0.06	(4.7 ± 0.2) × 10 <sup>-12</sup>	-30.3
N	-0.07	14.5			<6 × 10 <sup>-15</sup>	
H <sup>b</sup>	0.75	13.6			(2.2 ± 0.6) × 10 <sup>-11</sup>	-69.3

<sup>a</sup> Electron affinities and ionization potentials from refs 29 and 30. <sup>b</sup> Reference 31.

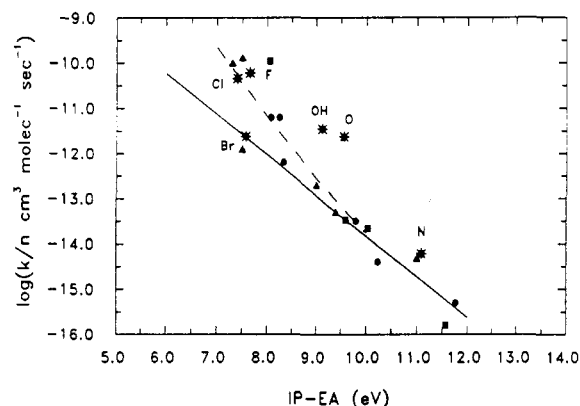


Figure 9. IP - EA plot for the X + ClNO (■), X + O<sub>3</sub> (▲), X + Cl<sub>2</sub> (●), and X + ClOCl (\*) reactions. The dashed line is a fit to the ClNO, O<sub>3</sub>, and Cl<sub>2</sub> data, while the solid line excludes X = Cl and F reactions.

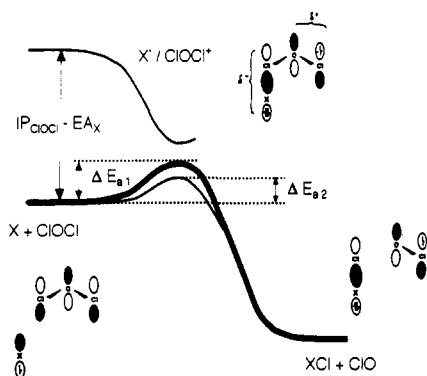


Figure 10. Schematic potential energy surfaces and frontier orbital interactions for X + ClOCl → XCl + ClO. The higher electron affinity of X increases the interaction of the X<sup>-</sup>/ClOCl<sup>+</sup> ionic surface (upper curve) with the ground-state adiabatic surface (heavy curve). This interaction lowers the reaction barrier from ΔE<sub>a1</sub> to ΔE<sub>a2</sub>.

the X = Cl and F reactions (see below). A frontier orbital picture of the delocalization of electron density from ClOCl to X appears in Figure 10. On the basis of ab initio calculations at the UHF/6-31G\* level of theory,<sup>27</sup> the HOMO for ClOCl is the doubly occupied B1 antibonding orbital, pictured in Figure 10. In the IP - EA model, the rate of reaction is controlled by the ease of electron delocalization and the reactants' ability to accommodate the partial charge separation that occurs as a result of the shift in electron density. This ability is reflected by the interaction of the low-lying ionic charge-transfer surface with the ground-state adiabatic surface (Figure 10).

For a homologous series, the value IP - EA reflects the proximity of the ionic surface to the ground-state surface at the transition state.<sup>1</sup> When this value is small, in addition to reflecting the ease of electron movement, it implies that the ionic surface lies relatively low in energy. This results in greater mixing of the

ionic state with the ground state in the region of the transition state. This perturbation lowers the intrinsic barrier to reaction by enhancing electron delocalization and stabilizing the polar transition state that results from the electron transfer (Figure 10). When the value of IP - EA is large, mixing with the ionic surface becomes less favorable as the energy gap between the surfaces increases. As a result, reactions at this end of the trend are largely covalent.

It is clear from Figure 9 that the reactions of Br, Cl, F, and N with ClOCl are consistent with the IP - EA trend of reactivity, suggesting that the rates for these reactions are determined by the ability of the reactants to enhance electron delocalization. The A factor and E<sub>a</sub> for reaction 1 are consistent with the experimental A factors and activation energies for the Br + ClNO<sup>1</sup> and O<sub>3</sub><sup>2</sup> reactions, again suggesting that the mechanisms for these reactions are similar. The small negative activation energy measured for reaction 2 has been seen before in the measurement of the Cl + ClNO reaction ( $k = (6.6 \pm 1.2) \times 10^{-11} \exp[(128 \pm 46)/T]$  cm<sup>3</sup> molec<sup>-1</sup> s<sup>-1</sup>),<sup>1</sup> as well as the Cl + OClO reaction ( $A = 3.0 \times 10^{-11}$  cm<sup>3</sup> molec<sup>-1</sup> s<sup>-1</sup>,  $E_a/R = 170$  K).<sup>28</sup> These reactions are too fast for the negative activation energy to be explained by the formation of a long-lived intermediate. It has been postulated that the negative temperature dependence for the Cl + ClNO reaction is due to the looseness of the Cl-ClNO transition state in a direct mechanism.<sup>1</sup> The large A factors for all three of these reactions support this hypothesis. The A factor and E<sub>a</sub> for reaction 3 are consistent with that for the F + ClNO reaction.<sup>1</sup> The large A factors and extremely small activation energies also suggest loose transition states for these F reactions; however, the reduced repulsion effects in the fluorine reactions result in a somewhat tighter transition state and thus a nonnegative activation energy.

The rate constants for the X = Cl and F reactions are significantly higher than the corresponding reactions for X = Br, even though the values of IP - EA are similar. This discrepancy may be due to the fact that the <sup>2</sup>P<sub>1/2</sub> excited state for Cl and F is accessible at room temperature (2.5 and 1.2 kcal/mol above the ground state)<sup>7</sup> and that the deviation from the trend may reflect the different reactivities of the ground and excited states. Bromine atom reactions would not show this deviation because the <sup>2</sup>P<sub>1/2</sub> state is not energetically accessible at room temperature. The enhanced rate constants of the Cl and F reactions would imply that the rate constant of the excited state is greater than that of the ground state, resulting in a weighted average of the two rate constants. However, the rate constants for the reactions of the <sup>2</sup>P<sub>1/2</sub> state with these molecules are unknown and may be smaller than the rate constants for the ground-state reactions. Because the rate constants for the reactions of Cl and F with both ClNO and ClOCl are extremely large, the contribution of the excited spin state to these rate constants at room temperature is probably negligible. More likely, the slower rates for X = Br may reflect the lower IP of this atom relative to Cl and F. The IP of Br is somewhat closer to the values of ClNO, O<sub>3</sub>, and ClOCl, and

(28) Toohey, D. W. Ph.D. Thesis, Harvard University, 1988.

(29) Hotop, H.; Lineberger, W. C. *J. Phys. Chem. Ref. Data* 1975, 4, 539.

(30) Franklin, J. L., et al. *Ionization Potentials, Appearance Potentials, and Heats of Formation of Gaseous Positive Ions*; National Standard Reference Data Series NSRDS-NBS26; U.S. Department of Commerce: Washington, D.C., 1969.

(31) Freeman, C. G.; Phillips, L. F. *J. Phys. Chem.* 1968, 72, 3031.

(27) Ab initio calculations were performed on: GAUSSIAN82 (release H); Binkley, J., Frisch, M., Raghavachari, K., Defrees, D., Schlegel, H., Whiteside, R., Fluder, E., Seeger, R., Pople, J. A., Eds.; Carnegie-Mellon University: Pittsburgh, PA, 1982.

therefore the rate constant may reflect the additional effect of electron transfer from Br back to the molecule. This effect would tend to reduce the rate of reaction, as electron delocalization from ClOCl to Br becomes more difficult.

The measured upper limit for the reaction of N with ClOCl is consistent with the upper limit reported for the N + O<sub>3</sub> reaction ( $<1 \times 10^{-15} \text{ cm}^3 \text{ molecule}^{-1} \text{ s}^{-1}$ )<sup>32</sup> and the room-temperature rate constants of N with Cl<sub>2</sub><sup>33</sup> and ClNO.<sup>1</sup> However, the high-temperature upper limit for the rate constant of N + ClOCl is not consistent with the *A* factor for the reaction of N + ClNO ( $A = (9.2 \pm 2.2) \times 10^{-12} \text{ cm}^3 \text{ molecule}^{-1} \text{ s}^{-1}$ ). Assuming that the *A* factors for these two reactions are similar, the high-temperature limit for the ClOCl reactions implies a room-temperature rate constant on the order of  $1 \times 10^{-17} \text{ cm}^3 \text{ molecule}^{-1} \text{ s}^{-1}$ , which falls well below that expected by the trend. Since the ionization potentials for ClOCl and ClNO are similar, on the basis of this model their reactivities should be similar. It is possible that the N + ClNO reaction produces N<sub>2</sub>O and Cl, analogous to the N + NO<sub>2</sub> → N<sub>2</sub>O + O reaction. The *A* factor and activation energy for the N + ClNO reaction may not reflect the reactivity of the Cl abstraction channel, and the agreement with the IP – EA trend may be fortuitous. However, there are little data on the temperature dependences for N radical–molecule reactions, so it is difficult to make any assumptions on the *A* factors for these reactions. As predicted by the IP – EA mechanism, the rate constants for these reactions are the smallest in the series, where the trend is poorly defined.

Table VII also includes kinetic, electronic, and thermodynamic data for the H + ClOCl → HCl + ClO reaction.<sup>31</sup> As seen for the reactions of H with ClNO<sup>1</sup> and O<sub>3</sub>,<sup>2</sup> these H atom reactions are anomalies because the rate constants are faster than predicted by the trend. Because most of the electron density in the HCl product resides on the Cl end of the molecule, it is likely that the electron delocalization occurs from H to ClOCl even though the IP of H (13.6 eV) is greater than the IP of ClOCl. From the large exothermicity, it is likely that the electron delocalization in this anomalous reaction is driven by thermochemistry.

The similar exothermicities of the Cl abstraction channels for the ClOCl reaction series would seem to suggest that the ground-state potential-energy surfaces for these reactions are similar. As demonstrated above, the differences in reactivity for the reactions of Br, Cl, F, and N with ClOCl can be explained using the IP – EA model. However, the room-temperature rate constants for the reactions of O and OH with ClOCl are not consistent with the IP – EA trend of reactivity, with the rates of these reactions several orders of magnitude faster than predicted from the trend. This seems to suggest that the potential-energy surfaces for these reactions are more complex than those for the other reactions in the series and may involve long-range attractive forces leading to stable intermediates. Explanations of the rate enhancements for these reactions are discussed in detail below.

**O + ClOCl → ClO + ClO.** The experimental room-temperature rate constant for reaction 4 is almost 2 orders of magnitude faster than that predicted from the IP – EA trend. The *A* factor for this reaction is consistent with the *A* factors for both the O + ClNO ( $k = (8.3 \pm 0.9) \times 10^{-12} \exp[(-1520 \pm 26)/T] \text{ cm}^3 \text{ molecule}^{-1} \text{ s}^{-1}$ ,  $k_{298} = (5.1 \pm 0.1) \times 10^{-14} \text{ cm}^3 \text{ molecule}^{-1} \text{ s}^{-1}$ ) and the O + O<sub>3</sub> reactions ( $A = 8.0 \times 10^{-12} \text{ cm}^3 \text{ molecule}^{-1} \text{ s}^{-1}$ ,  $E_a/R = 2060 \text{ K}$ ). However, the activation energy for the O + ClOCl reaction is over a factor of 2 smaller than that for the analogous reactions, even though the ionization potentials for the three species are very similar (IP(ClNO) = 10.9 eV,<sup>34</sup> IP(O<sub>3</sub>) = 11.7 eV<sup>30</sup>).

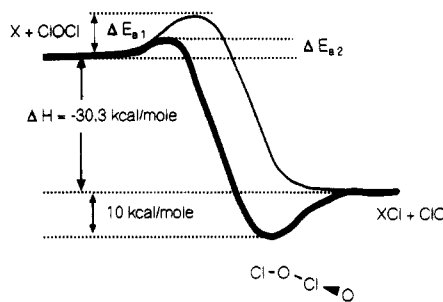
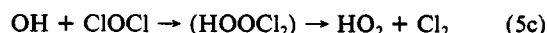


**Figure 11.** Schematic potential-energy surface (heavy curve) for the O + ClOCl → ClO + ClO reaction showing the effect of the ClOClO intermediate on the barrier to reaction. The presence of this intermediate results in a lower barrier ( $\Delta E_{a2}$ ) relative to that defined by the X + ClOCl surface ( $\Delta E_{a1}$ ) for the other reactions in this series which have similar exothermicities.

The lower activation energy (and subsequent rate enhancement) for the O + ClOCl reaction can be explained by the presence of a long-range attractive potential along the ground-state potential-energy surface forming the asymmetric ClO dimer (Figure 11). The stability of this form of the dimer has been calculated to be approximately 10 kcal/mol relative to ClO using ab initio theory (MP2/6-31G\*/UHF/6-31G\*).<sup>28</sup> The presence of this well in the exit channel for this reaction is consistent with the observed kinetic parameters. The positive activation energy for this reaction suggests that the lifetime of the intermediate is short relative to the rate of formation of the ClO products and that the first transition state is rate limiting. This is not surprising given the large exothermicity of the reaction to the formation of the ClO products. However, the existence of this intermediate results in a ground-state potential-energy barrier for the O + ClOCl reaction that is substantially lower than that for the other reactions in the series. This low barrier results in an overall rate of reaction which is faster relative to the IP – EA trend. The barrier may be further stabilized by interaction with the O<sup>-</sup>/ClOCl<sup>+</sup> ionic surface; however the ground-state barrier for this reaction is probably too low for mixing with the upper ionic state to occur.

**OH + ClOCl → Products.** Although the observation of a negative temperature dependence does not rule out a direct abstraction mechanism, the unusually large negative activation energy, coupled with a strong pressure dependence for the OH + ClOCl reaction, implies that the mechanism is more complex than a simple abstraction. A similar temperature dependence was observed by Poulet et al. for OH + OCIO → HOCl + O<sub>2</sub>.<sup>35</sup> To explain the observed negative temperature dependence of the OH + OCIO reaction and the observation of HOCl as the major product, a complex mechanism involving a cyclic intermediate was proposed. A similar intermediate would explain the observed temperature and pressure dependences for the OH + ClOCl reaction. The three thermodynamically allowed channels for this reaction suggest the possibility of two intermediate structures for a indirect mechanism:



For an indirect mechanism, the first two channels would involve a cyclic HOClOCl intermediate, while the third channel would involve attack of the oxygen of OH on the central oxygen atom of ClOCl. Channel 5a could also be the result of a direct mechanism.

If there were two distinct mechanisms for channels 5a and 5b (direct and indirect), one might expect the Arrhenius plot to reflect this and show significant curvature, as was observed for the OH + ClNO reaction.<sup>1,36</sup> If the Cl abstraction channel were direct,

(32) Except where noted, rate constant data are from: Demore, W. B.; Sander, S. P.; Golden, D. M.; Molina, M. J.; Hampson, R. F.; Kurylo, M. J.; Howard, C. J.; Ravishankara, A. R. *Chemical Kinetics and Photochemical Data for Use in Stratospheric Modeling: Evaluation Number 9*; JPL Publication 90-1; Jet Propulsion Laboratory: Pasadena, CA, 1990.

(33) Baulch, D. L.; Duxbury, J.; Grant, S. J.; Montague, D. C. *J. Phys. Chem. Ref. Data* **1981**, *10*, Suppl. 1.

(34) Alderice, D. S.; Dixon, R. N. *J. Chem. Soc., Faraday Trans. 2* **1977**, *73*, 245.

(35) Poulet, G.; Zagogianni, H.; LeBras, G. *Int. Chem. Kinet.* **1986**, *18*, 847.

(36) Finlayson-Pitts, B. J.; Ezell, M. J.; Wang, S. Z.; Grant, C. E. *J. Phys. Chem.* **1987**, *91*, 2377.

the temperature dependence for this channel probably would be positive and dominate the overall rate at high temperature (by analogy to the other reactions in the X + ClOCl series). The contribution of the direct channel to the overall rate could be estimated using the IP – EA trend. However, the absence of curvature toward a positive activation energy at higher temperatures for the OH + ClOCl reaction implies that a direct mechanism is probably not occurring, and therefore the IP – EA trend cannot be used to estimate the contribution of the Cl abstraction to the overall rate constant.

Similar temperature and pressure dependences have been observed for the OH + CO<sup>37</sup> and OH + HNO<sub>3</sub><sup>38</sup> reactions, the OH + OClO reaction mentioned above, and the ClO + HO<sub>2</sub> reaction.<sup>39</sup> Although it may be possible to explain the observed negative temperature dependence with a single transition state and a low energy barrier (similar to the Cl + ClOCl reaction above), the relatively large negative activation energy and pressure dependence suggest a mixed bimolecular/termolecular potential-energy surface for the OH + ClOCl reaction involving a strongly bound intermediate and two distinct transition states,<sup>40</sup> pictured in Figure 12. In this model, the observed negative temperature dependence implies that the second transition state is tighter and more stable than the first. Thus the density of states is higher for the first transition state, and at higher temperatures the observed rate constant decreases as dissociation into reactants becomes more favorable than formation of products (since the unimolecular rate constant in RRKM theory is proportional to the density of states in the transition state).<sup>40</sup> The observed pressure dependence implies that the lifetime of the intermediate is long relative to the formation of the bimolecular products, and thus the intermediate is probably strongly bound with respect to reactants. However, further low-temperature/high-pressure experiments, such as the pressure dependence of the product yield, are required in order to confirm this mixed bimolecular/termolecular mechanism. In addition, ab initio calculations of the intermediate structure and transition states, used in conjunction with a double-transition-state model, would be valuable in the understanding of the mechanism of this reaction.

Similar to the O + ClOCl reaction, the substantial rate enhancement of the OH + ClOCl reaction over that predicted from the IP – EA model can be attributed to the intermediate well along the potential-energy surface. The presence of this well results in a lower ground-state barrier for OH + ClOCl relative to the other reactions in the X + ClOCl series which follow the IP – EA trend and have similar exothermicities. As for the O + ClOCl reaction, the ground-state barrier for OH + ClOCl may be too low in energy relative to the upper ionic surface for mixing of these states to occur. Thus this reaction is probably dominated by covalent interactions.

### Trend Implications

The observed deviations of the reactions of O and OH with ClOCl bring the predictive power of the IP – EA trend into question. For these reactions, the experimental rate constants are several orders of magnitude larger than those predicted from the trend. However, this loss of predictive power is balanced by the valuable mechanistic insight gained from the trend comparisons. For the reactions of Br, Cl, F, and N with ClOCl, the consistency of the rate constants with the trend implies that the mechanism for these four reactions involves the delocalization of an electron from ClOCl to X in the abstraction of a Cl atom and that the activation energy depends on the ability of the transition state to accommodate the shift in electron density. The strength of this

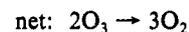
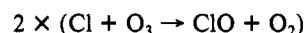
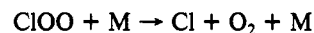
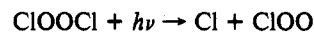
trend indicates that this mechanism may be common for non-hydrogen abstractions and perhaps is a fundamental interaction for all atom abstraction reactions. However, since the reactivities of O and OH are significantly faster than predicted from the IP – EA trend comparison, the mechanisms of these reactions must be more complex than a simple delocalization of electron density.

It has been observed that positive deviations from the IP – EA trend defined by the reactions of X with ClNO, O<sub>3</sub>, and XY occur for reactions involving long-range attractive potentials, such as recombination, dipole–dipole interactions, or dipole-induced dipole interactions.<sup>28</sup> These effects tend to reduce the activation energy for reaction, and thus the overall rate constant is enhanced relative to that predicted from the IP – EA trend analysis. Negative deviations occur for reactions involving more complex species, where the mechanisms may involve orbitals other than the frontier orbitals which define the IP and EA of the reactants.<sup>41</sup>

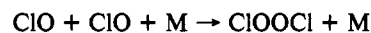
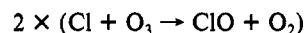
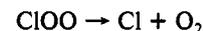
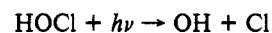
By comparing the room-temperature rate constants for atom abstractions by small radicals to those estimated from the IP – EA trend, one can deduce whether the reactions proceed by direct abstraction, controlled by the ease of electron delocalization, or by more complex mechanisms which may involve long-range potentials or intermediates. The IP – EA trend serves as a benchmark for the mechanistic understanding of these reactions. This comparison can yield new insight into the reactivity of complex systems and motivate future experiments and theoretical calculations designed to further define the potential-energy surfaces of these reactions.

### Appendix: Atmospheric Implications

Although the reactions of ClOCl are not directly involved in the chemistry of the atmosphere, because of the similarity in structure and reactivity of the ClO dimer (ClOOC) to ClOCl, the reactions of the ClO dimer may be estimated based on the reactivity of ClOCl. The ClO dimer plays an important role in polar chemistry and is directly involved in the mechanism of ozone destruction within the enhanced ClO regions of the antarctic stratosphere:<sup>8–10</sup>



An alternative mechanism involves the reaction of OH with ClOOC:



Thus it is important to examine the chemistry of the ClO dimer in order to understand what effect the kinetics of this species might have on mechanisms of ozone destruction.

Although the rate constant for the OH + ClOOC reaction has yet to be measured, the room-temperature rate constants for Br + ClOOC and Cl + ClOOC have been measured ( $k_{298} = 3 \times 10^{-12}$  and  $1 \times 10^{-10}$  cm<sup>3</sup> molecule<sup>-1</sup> s<sup>-1</sup>, respectively).<sup>32</sup> The similarity of these rate constants with the room-temperature rate constants of Br and Cl with ClOCl suggest that the rate constant for the reaction of OH with ClOOC may be as large as that for the OH + ClOCl reaction, since it is likely that the mechanisms for Cl abstractions from ClOCl and ClOOC are similar. It is also reasonable to assume that the mechanism for the OH +

(37) See for example: Smith, J. W. M.; Zellner, R. *J. Chem. Soc., Faraday Trans. 2* 1973, 69, 1617. Baulch, D. L.; Cox, R. A.; Humpson, R. F., Jr.; Kerr, J. A.; Troe, J.; Watson, R. T. *J. Phys. Chem. Ref. Data* 1980, 9.

(38) See for example: Connell, P. S.; Howard, C. J. *Int. J. Chem. Kinet.* 1985, 17, 17. Margitan, J. J.; Watson, R. T. *J. Phys. Chem.* 1982, 86, 3819.

(39) Stimpfle, R. M.; Perry, R. A. A.; Howard, C. J. *J. Chem. Phys.* 1979, 71, 5183.

(40) See for example: Patrick, R.; Barker, J. R.; Golden, D. M. *J. Phys. Chem.* 1984, 88, 128. Kirchner, C. C.; Sander, S. P. *J. Phys. Chem.* 1984, 88, 2082. Mozurkewich, M.; Benson, J. W. *J. Phys. Chem.* 1984, 88, 6429.

(41) Abbatt, J. P. D.; Anderson, J. G. *J. Phys. Chem.* 1991, 95, 2382.

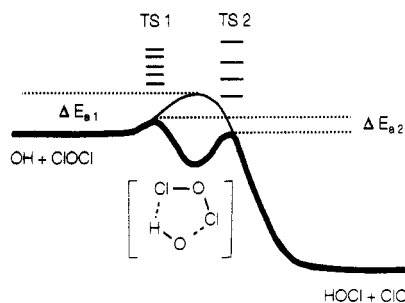
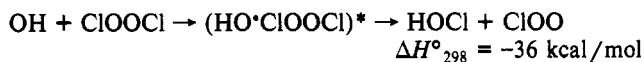


**Figure 12.** Schematic potential-energy surface (heavy curve) for the  $\text{OH} + \text{ClOOCl} \rightarrow \text{products}$  reaction showing the effect of a stable  $\text{HOClOCl}$  intermediate on the barrier to reaction. The presence of this intermediate results in a lower reaction barrier ( $\Delta E_{a2}$ ) relative to the barrier defined by the  $\text{X} + \text{ClOOCl}$  surface for the other reactions in the series ( $\Delta E_{a1}$ ). The observed negative activation energy for this reaction implies two distinct transition states, with the second transition state tighter and more stable than the first (see text).

$\text{ClOOCl}$  reaction may also proceed via a stable  $\text{OH}\cdot\text{ClOOCl}$  intermediate, similar to the  $\text{OH}\cdot\text{ClOOCl}$  intermediate proposed here:



Thus the rate constant for  $\text{OH} + \text{ClOOCl}$  reaction may also exhibit a negative temperature dependence. The question becomes whether this large rate constant for the  $\text{OH} + \text{ClOOCl}$  reaction results in a rate at antarctic temperatures which competes with the photolysis rate of  $\text{ClOOCl}$ . A fast rate for the  $\text{OH} + \text{ClOOCl}$  reaction would shift the catalytic destruction of ozone from one involving  $\text{ClO}$  dimer photolysis (mechanism I) to one involving  $\text{HOCl}$  photolysis (mechanism II).

In order to determine what effect the  $\text{OH} + \text{ClOOCl}$  reaction might have on mechanisms of ozone destruction, the  $\text{OH} + \text{ClOOCl}$

rate constant was used in a zero-dimensional photochemical kinetic simulation<sup>42</sup> as a surrogate for the rate constant for the  $\text{OH} + \text{ClOOCl}$  reaction. The model was run from 25 August to 1 September, at 65°S, 20 km, and 210 K. The initial conditions simulated the antarctic stratosphere just prior to destruction of ozone; preprocessed air (where  $\text{NO}_x$  is removed by heterogeneous reactions with polar stratospheric clouds), with elevated concentrations of  $\text{ClO}_x$  ( $[\text{ClO}] + [\text{ClOOCl}] = 3 \times 10^9 \text{ cm}^{-3}$ ), and midlatitude concentrations of  $\text{HO}_x$  ( $[\text{OH}]$  and  $[\text{HO}_2] = 1 \times 10^6 \text{ cm}^{-3}$ ).

The results of the model reveal that, with midlatitude values of  $\text{HO}_x$ , the  $\text{OH} + \text{ClOOCl}$  reactions is over 200 times slower than the photolysis of  $\text{ClOOCl}$  and, as a result, has no significant effect on calculated ozone destruction rates. However, confirmation of these results awaits the direct measurement of the  $\text{OH} + \text{ClOOCl}$  reaction rate constant, and in situ measurements of  $\text{HO}_x$  in the antarctic stratosphere. If the polar concentrations of  $\text{HO}_x$  were significantly higher, the  $\text{OH} + \text{ClOOCl}$  reaction may begin to compete with the photolysis of the  $\text{ClO}$  dimer. The  $\text{OH} + \text{ClOOCl}$  reaction would begin to slowly partition active chlorine from  $\text{ClOOCl}$  to  $\text{HOCl}$ , and the destruction of ozone would become limited by  $\text{HOCl}$  photolysis. The overall rate of the  $\text{OH} + \text{ClOOCl} \rightarrow \text{HOCl} + \text{ClO}$  reaction is, however, constrained by observations of  $\text{HOCl}$  abundances.<sup>43</sup>

**Acknowledgment.** We thank P. O. Wennberg for experimental assistance and S. A. Lloyd and D. E. Anderson for use of their photochemical model and acknowledge helpful discussions with W. H. Brune. This work was supported by the National Science Foundation, Grant ATM-8601126.

**Registry No.**  $\text{COCl}$ , 7791-21-1;  $\text{Br}$ , 10097-32-2;  $\text{Cl}$ , 22537-15-1;  $\text{F}$ , 14762-94-8;  $\text{O}$ , 17778-80-2;  $\text{N}$ , 17778-88-0;  $\text{OH}$ , 3352-57-6.

(42) Anderson, D. E.; Lloyd, S. A. *J. Geophys. Res.* **1990**, *95*, 7429.

(43) Toon, G. C.; Farmer, C. B. *Geophys. Res. Lett.* **1989**, *16*, 1375.

## Intramolecular Photochemical Electron Transfer. 7. Temperature Dependence of Electron-Transfer Rates in Covalently Linked Porphyrin-Amide-Quinone Molecules<sup>1</sup>

Jing-yao Liu and James R. Bolton\*

*Photochemistry Unit, Department of Chemistry, The University of Western Ontario, London, Ontario, Canada N6A 5B7 (Received: May 8, 1991; In Final Form: October 14, 1991)*

Intramolecular rate constants  $k_{\text{ET}}$  for electron transfer (ET) from a porphyrin excited singlet  $S_1$  state to a linked quinone acceptor have been measured as a function of temperature in several solvents for the molecule PAQ [5,10,15-trityl-15-(4-carboxylphenyl)porphine linked to *p*-benzoquinone via an amide group]. Most of the data could be analyzed successfully using the high-temperature form of the semiclassical Marcus equation. The analysis of temperature dependence data allows the separation of the electronic and nuclear factors in the Marcus equation. The results indicate that both factors are solvent dependent. The electronic factor, involving the electronic coupling energy  $H_{\text{ep}}$ , is found to have larger values in polar solvents and smaller values in most nonpolar solvents. On the other hand, the nuclear factor is not found to correlate with solvent polarity. The analysis of the temperature dependence of  $k_{\text{ET}}$  provides a plausible explanation for the scatter found in a former analysis of solvent effects for photoinduced electron transfer in PAQ.

### Introduction

Electron transfer (ET) reactions<sup>2</sup> are among the most common and fundamental processes in chemistry and biochemistry. Since the development of the theory of electron transfer by Marcus and

others,<sup>3-5</sup> this subject has been an area of lively investigation. In particular, over the past 12-14 years there has been a growing interest in the study of intramolecular ET in molecules where a donor and an acceptor are covalently linked; these systems have proved to be a fruitful testing ground for systems designed to mimic

(1) Contribution No. 441, Photochemistry Unit, Department of Chemistry, The University of Western Ontario.

(2) For reviews, see: (a) Sutin, N.; Marcus, R. A. *Biochim. Biophys. Acta* **1985**, *811*, 265. (b) Bolton, J. R.; Archer, M. D. In *Electron Transfer in Inorganic, Organic and Biological Systems*; Bolton, J. R., Mataga, N., McLendon, G. L., Eds.; Advances in Chemistry Series 228; American Chemical Society: Washington, DC, 1991; Chapter 2, pp 7-23.

(3) Marcus, R. A. (a) *J. Chem. Phys.* **1956**, *24*, 966; (b) *Faraday Discuss. Chem. Soc.* **1960**, *29*, 21; (c) *Annu. Rev. Phys. Chem.* **1964**, *15*, 155; (d) *J. Chem. Phys.* **1965**, *43*, 679.

(4) Levich, V. G.; Dogonadze, R. R. *Collect. Czech. Chem. Commun.* **1961**, *26*, 193.

(5) Kestner, N. R.; Lofan, J.; Jortner, J. *J. Phys. Chem.* **1974**, *78*, 2148.